Analysis and Thermal Property Investigations into Ternary Actinide Chloride Salt Systems Containing UCl₃ and PuCl₃

August 2023

Toni Karlsson, Michael Woods, Robin Roper
Advanced Technology of Molten Salts

Mark Lounsbury
Fuel Fabrication Facility Operations

Nick Erfurth
Analytical Laboratory

Stephen Warmann, David Tolman
Pyrochemistry & Molten Salt Systems

INL Idaho National Laboratory

Analysis and Thermal Property Investigations into Ternary Actinide Chloride Salt Systems Containing UCl$_3$ and PuCl$_3$

Toni Karlsson, Michael Woods, Robin Roper
Advanced Technology of Molten Salts
Mark Lounsbury
Fuel Fabrication Facility Operations
Nick Erfurth
Analytical Laboratory
Stephen Warmann, David Tolman
Pyrochemistry & Molten Salt Systems

August 2023

Idaho National Laboratory
Advanced Technology of Molten Salts, C440
Idaho Falls, Idaho 83415

http://www.inl.gov

Page intentionally left blank

INL ART Program

Analysis and Thermal Property Investigations into Ternary Actinide Chloride Salt Systems Containing UCl$_3$ and PuCl$_3$

INL/RPT-23-74483
Revision 0

August 2023

Technical Reviewer: (Confirmation of mathematical accuracy, and correctness of data and appropriateness of assumptions.)

_____   ___8-30-23___
Guy Fredrickson   Date
Research Scientist

Approved by:

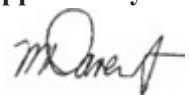_____   8/31/2023
Michael E. Davenport   Date
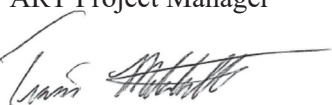ART Project Manager

_____   8/31/2023
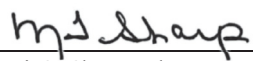Travis R. Mitchell   Date
ART Program Manager

_____   8/31/2023
Michelle T. Sharp   Date
INL Quality Assurance

Page intentionally left blank

SUMMARY

While literature data on the thermal properties of clean fuel salts is lacking, even less data is available on the properties of fuel salts containing impurities. This information is crucial to regulators, MSR developers, and the scientific community alike. It is essential to understand, benchmark, and predict crucial data on the changes in thermal properties of fuel salt systems due to impurities arising from moisture, corrosion, and reactor operation (i.e., fission products). This research focuses on two actinide fuel salts (1) to investigate a worst-case scenario buildup of actinide fission product in a NaCl-UCl$_3$ eutectic fuel salt and (2) to investigate NaCl-PuCl$_3$ eutectic fuel salt after 1,000 hr of operation in a natural circulation flow loop to determine if corrosion or atmospheric (moisture/oxygen) products are present. For the first salt, a conservative assumption or worst-case scenario for fission product buildup was investigated by adding PuCl$_3$ to 67NaCl–33UCl$_3$ (mol%) eutectic salt, resulting in a ternary salt having a composition of 61NaCl–30UCl$_3$–9PuCl$_3$ (mol%) Addition of PuCl$_3$ to NaCl-UCl$_3$ eutectic resulted in a ternary salt with a higher melting temperature than either the NaCl-PuCl$_3$ or NaCl-UCl$_3$ binary eutectic mixtures. Addition of PuCl$_3$ also resulted in an increase in density, which was expected. The second salt was extracted from a micro loop. The composition of the fuel (primary) salt prior to flow loop operations was determined to be 64NaCl–36PuCl$_3$ (mol%); however, analyses of the post-flow loop salt showed increased levels of MgCl$_2$ and NaCl, changing the salt composition to 10MgCl$_2$–64NaCl–26PuCl$_3$ (mol%), indicating the primary salt interacted with the rinse salt (NaCl-MgCl$_2$). Analysis of the post-flow loop salt detected low concentrations of Al, Ni, Co, Nb, and Zr, most likely corrosion products from the materials of construction. Contamination of the fuel salt with the rinse salt decreased the density by approximately 10% and reduced the onset melting temperature by 50°C, from 451°C to approximately 400°C. Results from the fission product simulated salt (61NaCl–30UCl$_3$–9PuCl$_3$ (mol%)) and the corrosion product salt (10MgCl$_2$–64NaCl–26PuCl$_3$ (mol%)) will be included in two separate future manuscripts.

Page intentionally left blank

TABLE OF CONTENTS

FIGURES

TABLES

ACRONYMS

AFCI   Advanced Fuel Cycle Initiative

AIMD   Ab-Initio Molecular Dynamics

ARL   Analytical Research Laboratory

ASTM   American Standard Test Method

DSC   Differential Scanning Calorimeter

FCF   Fuel Conditioning Facility

FMF   Fuel Manufacturing Facility

FY   Fiscal Year

ICP-MS   Inductively Coupled Plasma – Mass Spectrometry

ICP-OES   Inductively Coupled Plasma – Optical Emission Spectrometry

INL   Idaho National Laboratory

MSR   Molten Salt Reactor

NIST   National Institute of Standards and Technology

NRC   Nuclear Regulator Committee

PNNL   Pacific Northwest National Laboratory

S&CL   Standards and Calibration Laboratory

STA   Simultaneous Thermal Analyzer

TEVA   Tetra Valent Actinides

TGA   Thermogravimetric Analysis

Page intentionally left blank

Analysis and Thermal Property Investigations into Ternary Actinide Chloride Salt Systems Containing UCl$_3$ and PuCl$_3$

1.   INTRODUCTION

Despite the current development of advanced molten-salt reactors (MSRs), regulators, MSR developers, and the scientific community still lack the understanding of, and access to, literature data on the behavior of clean fuel salts and how these behaviors change with the accumulation of impurities. Changes in the thermal properties of fuel salt can yield unforeseen changes in the three primary safety functions of the reactor, which are identified by the Nuclear Regulatory Commission (NRC) as (1) reactivity control, (2) heat removal from the reactor, and (3) confinement of radionuclides. For example, large drifts in thermal properties can cause lower reactivity-temperature feedback and a decrease in thermal conductivity of the fuel salt. Therefore, it is necessary to understand, benchmark, and predict crucial data on the changes in thermal properties of fuel salt systems due to impurities arising from moisture, corrosion, and reactor operation (i.e., fission product buildup). The three main impurity categories are described briefly in Table 1.

Table 1. Brief description of the three main impurity categories expected to be present in MSR fuel systems.

Moisture/Oxygen	Most common impurities because salts are very hygroscopic. Moisture reacts to form corrosive hydrogen cations (H$^+$), hydroxides (OH$^-$), oxyhalides, oxides, and hydrochloric (HCl) gas (Sridharan and Allen 2013). Metals, such as manganese (Mn), chromium (Cr), iron (Fe), and copper (Cu), typically found in materials of construction, become chlorinated in the presences of HCl gas, leading to corrosion, and their solubilities cause a change in salt composition.
Corrosion Products	Typically result from metal alloys containing high concentrations of Cr, silicon (Si), or aluminum (Al) normally added to materials of construction to suppress corrosion at high temperature through the formation of passive oxide films. However, in molten salts, the passive oxide layer does not form or is unstable (Raiman and Lee 2018).
Fission Products	Fission products in fuel salts and can be categorized into three classes: noble gases, soluble metals, and insoluble metals. The noble gases are predicted to be removed by a cover gas where the insoluble metals will deposit at the salt-gas interface and on metal surfaces such as containments and pumps (Compere et al. 1975). Soluble metals will remain in the salt, continually accumulating with burnup, and subsequently modifying the thermal properties. Therefore, soluble fission product buildup in salts is of high interest with respect to thermal properties.

The current work has two key goals for thermophysical property measurements: (1) study the extent to which impurity-driven variations, in this case a bounding scenario where transuranic fission products represented by plutonium chloride (PuCl$_3$) buildup in a 67 sodium chloride (NaCl)- 33 uranium chloride (UCl$_3$) (mol%) fuel salt and (2) examine the potential fuel salt 64NaCl-36PuCl$_3$ (mol%) after 1,000 hr of operation in a natural convection micro loop (TerraPower) to quantify corrosion products that may build up in the salt or cause reduction-oxidation reaction with fuel salt constituents, such as Pu.

Under the DOE MSR Campaign, several milestones were set for fiscal year (FY) 2023 and are listed in Table 2. This report satisfies milestone M3AT-23IN0705021, *Draft Journal Article on NaCl-UCl$_3$-*

PuCl₃ Properties, and describes the work completed thus far for milestone M3AT-23IN0705023, *Complete Chemical/Isotopic Analysis of FCF Flow Loop Salt*. The research included in this report will be used in two journal articles. The contents of Section 2 will be included in a joint manuscript with Dr. Manh Thuong Nguyen of Pacific Northwest National Laboratory (PNNL) with a tentative title, *"A Combined Computational Experimental Study of NaCl–UCl₃–PuCl₃ Molten Salt Mixtures."* The contents described in Section 3 will be included in a joint publication with TerraPower with a tentative title, "Analysis of an Actinide Fuel Salt and Micro-Loop after 1000 Hours of Micro-Loop Operating Hours." At this time, there has been no decision on where these journals will be submitted for publication.

Table 2. Idaho National Laboratory FY-23 work package milestones.

Milestone Number	Milestone Title	Due Date	Status	Report Section Reference
M3AT-23IN0705021	Draft Journal Article on NaCl-UCl₃-PuCl₃ Properties	September 15, 2023	Complete	Section 2
M3AT-23IN0705022	Retrieve Salt from FCF Hot Cell Facility and Initiate Chemical/Isotopic Analysis	July 14, 2023	Completed	Section 3
M3AT-23IN0705023	Complete Chemical/Isotopic Analysis of FCF Salt	February 15, 2024	On-time	Section 3

In addition to the research activities described in Sections 2 and 3 of this report, FY-23 funding also provided early career researchers with an opportunity to modify existing experimental setups and develop new techniques for high-temperature molten-salt property measurements and to optimize experimental parameters for collecting heat capacity and density data with lower uncertainty. During the execution of the FY-23 research activities, opportunities were utilized to mentor early career researchers (interns, post-doctoral researchers, and staff hires) on molten-salt thermophysical properties data acquisition and reporting. Participation in conferences, presentations (oral and poster), and professional networking was encouraged.

2.   TERNARY NaCl-UCl₃-PuCl₃ SALT

Using NaCl-UCl₃ as a fuel in MSRs has been discussed for decades and is actively being pursued by private industry. The current rapid societal shift toward renewable energies, mitigating climate change, and a push for carbon neutral energy sources has renewed interest in nuclear energy as a low-carbon footprint energy source (IAEA 2021). Advanced MSRs are one type of nuclear reactor design being considered today by several countries including the United States, Canada, China, France, South Korea, the Netherlands, Norway, and Denmark. Fuel compositions of actinide fluorides and chlorides are typically considered; however, a recent study on heavier halides indicates that bromide and iodine fuels may also be possible (Faure and Kooyman 2022). A limited amount of experimental thermophysical property data is available on the NaCl-UCl₃ fuel salt system; furthermore, little to no experimental data is available on salts containing corrosion products or increased concentrations of actinides, which could be present due to reactor operations and fuel burnup. A pseudo-binary salt where salt 1 is the 67NaCl-33UCl₃ eutectic and salt 2 is the PuCl₃, was investigated as a worst-case scenario for fuel burnup and in inclusion of actinide fission products on the changes in thermal properties.

2.1 Methods

All material handling and experimentation were performed in an inert atmosphere glovebox with oxygen and moisture levels maintained below 5 and 0.1 ppm, respectively. Physical measurements of all masses were made using a calibrated analytical balance. Balances are calibrated annually by the Standards and Calibration Laboratory (S&CL) at the Idaho National Laboratory (INL), and they are

assigned an uncertainty for their measurement range. Daily checks are performed on these balances using National Institute of Standards and Technology (NIST)-traceable external calibration weights, also calibrated by the S&CL, to confirm the balance functionality and accuracy before use.

2.1.1 Salt Blending

Non-radioactive salts components such as NaCl were heated under a 17.5 kPa absolute vacuum to 350°C for approximately 24 hr in an argon atmosphere glovebox to ensure the salt was free of moisture. $PuCl_3$ was added in the form of 64NaCl-36PuCl$_3$ (mol%) eutectic salt. The NaCl-PuCl$_3$ eutectic salt was well characterized and studied previously (Karlsson, Middlemas, et al. 2023). 5.413 g of NaCl, 8.324 g of NaCl-PuCl$_3$ eutectic, and 21.264 g of UCl$_3$ were used to make the ternary salt sample. The UCl$_3$ was available at INL. The resulting sample had a composition of 61NaCl-30UCl$_3$-9PuCl$_3$ (mol%).

To construct the salt mixture, each salt constituent was weighed and added to a glassy carbon crucible. The mixture was stirred and placed in a furnace. The sample was heated above the melting temperature to 700°C, forming a homogenous ternary salt. Once cooled, the salt was ground using an agate mortar and pestle to ensure homogeneity. Approximately, 1 g of the salt was held in reserve to determine the melting temperature at the Analytical Research Laboratory (ARL). The remaining salt, approximately 34 g, was used for density measurements and stored in a closed metal container until needed for thermal property measurements.

2.1.2 Salt Stability and Melting Point

Transition temperatures and enthalpies of transition were determined employing a simultaneous thermal analyzer (STA), Netzsch 449 F1, with differential scanning calorimeter (DSC)/thermogravimetric analyzer (TGA) type-S sample carrier. This instrument was located inside an argon atmosphere glovebox having oxygen and moisture levels below 5 ppm and 0.1 ppm, respectively. Glassy carbon crucibles (diameter 6 mm, 50 μl) and lids, rated to 2400°C, were used to contain the salt samples and calibration standards. There were no observable interactions between the glassy carbon crucibles and the salts. Crucible lids had a small hole in the center to prevent a buildup of pressure in the crucible by allowing the escape of off gases, if this were to occur.

Calibrating the STA for temperature and heat flow was performed using six high-purity standards, including indium (In), bismuth (Bi), zinc (Zn), aluminum (Al), silver (Ag), and gold (Au), for each of the three heating rates: 20, 10, and 2°C min^{-1}. The transition temperatures and enthalpy of the standards were calculated by averaging the onset and peak area for three heating cycles (ASTM 2018). Enthalpies of transition were determined by integrating the full area under each transition peak from the transition start to the transition finish. The temperature and sensitivity calibrations were accurate in the range of 164 to 1050°C by verification using a Zn standard (Table 3), where the experimental melting temperature was within ±1°C for each heating rate. The enthalpy of Zn at different heating rates was accurate to ±1%.

Table 3. Experimental STA results of zinc standard (run as sample) using the temperature and heat flow calibration files for multiple heating rates.

Heating Rate °C min^{-1}	Cycle 1 °C	Cycle 2 °C	Cycle 3 °C	Average °C	Deviation °C	Error %
20	420.2	420.4	420.3	420.3	0.10	0.19
10	419.9	420.0	420.2	420.0	0.15	0.13
2	419.3	419.3	419.5	419.4	0.12	0.03
°C min^{-1}	J g^{-1}	J g^{-1}	J g^{-1}	J g^{-1}	J g^{-1}	%
20	108.7	108.7	108.5	108.6	0.12	0.27
10	110.5	110.6	110.7	110.6	0.10	0.74

Heating Rate	Cycle 1	Cycle 2	Cycle 3	Average	Deviation	Error
2	111.6	111.6	111.4	111.5	0.12	0.96

2.1.3   Density

For density determination, the salt was loaded into a glassy carbon crucible previously cleaned with deionized water and isopropyl alcohol and baked in a furnace at 800°C for 2 hr. The glassy carbon crucible containing the salt was then placed in a Ventura Electromelt furnace modified for density experiments. Figure 1 shows the Archimedes densitometer setup within the glovebox including the furnace, stand, and bottom hanging balance and is described in greater detail by Duemmler et al. (Duemmler et al. 2022) and Karlsson et al. (Karlsson, Middlemas, et al. 2023). A nickel (Ni) bobber was tied onto the wire and its volume calculated in 10 mL of both deionized water and ethanol, which have well-defined densities near room temperature. The mass of the bobber and wire was then measured using the hang down balance (Mettler Toledo WXSS204, tolerance 0.8 mg). The crucible with salt, quartz lid, and bobber with wire was added to the setup, and the salt was melted.

Figure 1. Experimental density setup showing bottom-loading balance on the stand above a furnace with quartz lid and thermocouple inserted inside the Advanced Fuel-Cycle Initiative glovebox.

Mass readings were performed after 5 min of thermal stability at each temperature as measured by an Inconel-sheathed type-K thermocouple (OMEGA) inserted directly into the salt. This equilibration was on average 60 min after each temperature change of approximately 50°C. An internal adjustment of the balance was performed before each set of mass measurements at a unique temperature. The balance was tared before each measurement. Density measurements were taken between 550 and 860°C.

The density calculations were performed using the direct Archimedean method based on the measurement of buoyancy force exerted on a bobber submerged in molten salts. The density of the salt at an experimental temperature T is calculated by Equation (1), where m is the measured mass of the bobber and wire out of the salt (suspended in argon), w_{salts} is the measured mass of the bobber and wire suspended in the salt, g is the acceleration due to the gravity of Earth, α is the linear thermal coefficient of expansion of Ni, and T_0 is the reference temperature for V_0, the reference volume of the Ni bobber. The

linear thermal coefficient of expansion of Ni was calculated based on a polynomial fit of reference data (Hidnert 1957).

$$\rho_{salts} = \frac{m - w_{salts}}{V_0(1 + 3\alpha(T - T_0))} \tag{1}$$

The experimental uncertainty of the density was calculated by the propagation of individual uncertainties. Equation (2) shows the fundamental form of the uncertainty propagation of Equation (1). Equation (3) shows the simplified experimental uncertainty function, and Table 4 lists the individual uncertainties and their explanations.

$$\sigma_{\rho_{salt}}^2 = \left(\frac{\partial \rho_{salt}}{\partial m}\right)^2 \sigma_m^2 + \left(\frac{\partial \rho_{salt}}{\partial w_{salt}}\right)^2 \sigma_{w_{salt}}^2 + \left(\frac{\partial \rho_{salt}}{\partial V_0}\right)^2 \sigma_{V_0}^2 + \left(\frac{\partial \rho_{salt}}{\partial \alpha}\right)^2 \sigma_\alpha^2 + \left(\frac{\partial \rho_{salt}}{\partial T}\right)^2 \sigma_T^2 \tag{2}$$

$$\sigma_{\rho_{salt}} = \rho_{salt} \sqrt{\frac{\sigma_m^2 + \sigma_{w_{salt}}^2}{(m - w_{salt})^2} + \frac{\sigma_{V_0}^2}{V_0^2} + \frac{9\alpha^2(T - T_0)^2}{\left(1 + 3\alpha(T - T_0)\right)^2}\left(\frac{\sigma_\alpha^2}{\alpha^2} + \frac{\sigma_T^2}{(T - T_0)^2}\right)} \tag{3}$$

Table 4. Definition of terms used to calculate the error associated with liquid density measurements.

Symbol	Explanation
σ_m	Standard deviation of the five weight measurements out of salt
$\sigma_{w_{salt}}$	Standard deviation of the five weight measurements in salt
σ_{V_0}	Standard deviation of the two calculated volumes from water and ethanol benchtop trial
σ_α	Assigned as 1% of value of α
σ_T	OMEGA assigned 0.05% * T + 0.3°C

2.2 Results

2.2.1 Salt Blending

Figure 2A–C shows the individual chemicals that were combined to make the ternary salt. The NaCl-PuCl$_3$ eutectic salt (Figure 2C) was prepared for the MSR Campaign in FY-22 (Karlsson et al. 2022). The resulting homogenized, fused salt ingot is shown in Figure 2D–F. The bottom of the crucible was dark in color, while the top exposed surface was dark but showed some orange specks on the surface, indicating the possible presence of uranium oxides. The ingot material was homogenized and size-reduced with a mortar and pestle.
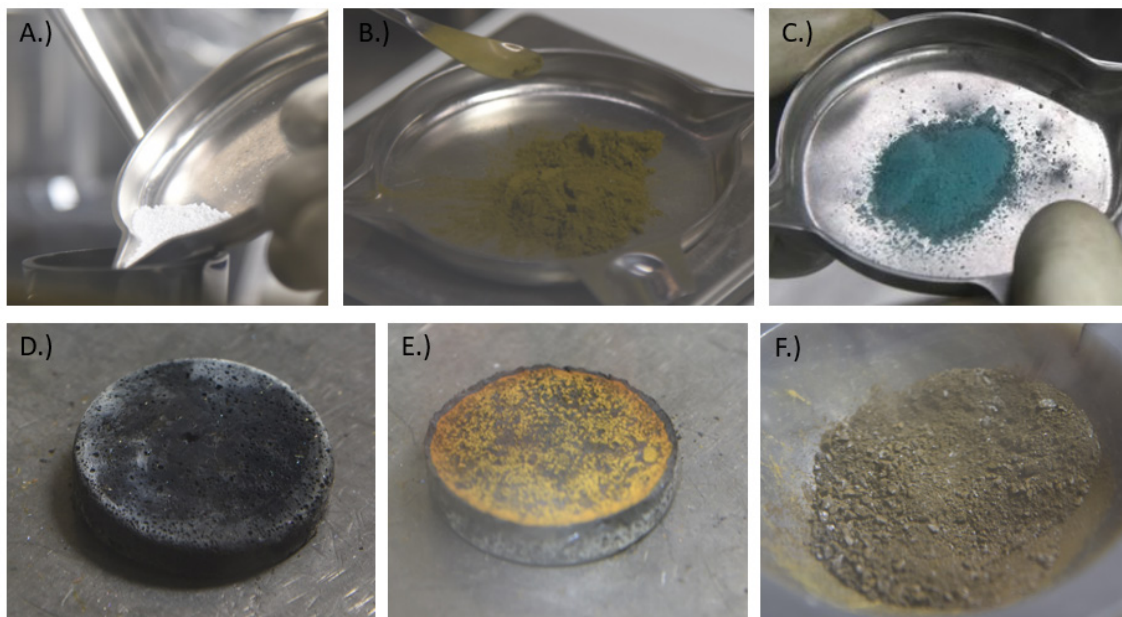
Figure 2. Chemicals and mixtures for making ternary 61NaCl–30UCl₃–9PuCl₃ (mol%). A.) NaCl, B.) UCl₃, C.) NaCl-PuCl₃ eutectic, D.) puck of ternary salt after heating (bottom), E.) puck of ternary salt after heating (top), and F.) size-reduced ternary salt.

During experimental preparations, the glassy carbon crucible used for homogenization and melting of the ternary salt was cleaned using ethanol. The crucible was not dried in a furnace after cleaning, and it is probable that some residual ethanol contaminated the salt and, upon heating, formed the orange uranium oxide compound seen in Figure 2E. UO_2 formation from a chloride media was reported by Vigier et al. (Vigier et al. 2016), according to Equation (4). Oxidation of UO_2 leads to the formation of U_3O_8 according to Equation (5). The yellow to orange compounds of UO_2, UO_3, and U_3O_8 have all been reported in literature (Thein and Bereolos 2000; Vigier et al. 2016). However, it was not feasible within this scope of work to characterize the orange-yellow compound.

$$UCl_{3(salt)} + 2H_2O_{(g)} = UO_{2(solid)} + 3HCl_{(g)} + 1/2H_{2(g)} \qquad (4)$$

$$3UO_{2(s)} + O_{2(g)} \xrightarrow{300-700°C} U_3O_{8(s)} \qquad (5)$$

6
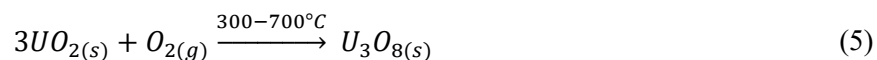
2.2.2   Melting Point

Both the NaCl-UCl$_3$ and NaCl-PuCl$_3$ salt systems are simple binaries with a single eutectic transition. The eutectic melting temperature of 67NaCl–33UCl$_3$ (mol%)has been reported to be 520°C (Sooby et al. 2015), while the eutectic melting temperature of 64NaCl–36PuCl$_3$ (mol%) has been reported to be 451°C (Karlsson, Middlemas, et al. 2023). The ternary salt thermograms for three heating rates (20, 10, 2°C min^{-1}) are shown in Figure 3. There are three peaks present and labeled in Figure 3, occurring at approximately 410°C (Peak 1, onset), 515°C (Peak 2), and 564°C (Peak 3, endset). Peak 3 represents the liquidus transition of the ternary mixture. Peak 2 likely represents the NaCl-UCl$_3$ eutectic transition. The underlying transition or phase change occurring at Peak 1 is unknown, but two hypotheses are (1) the presence of a low concentration of a uranium-oxide compound, such as UO$_2$, UO$_3$, or U$_3$O$_8$ (Thein and Bereolos 2000), or (2) the presence of Pu metal (Karlsson, Adkins, et al. 2023), has been shown to cause an unidentified transition in the NaCl-PuCl$_3$-Pu phase diagram at approximately 410°C. The NaCl-PuCl$_3$ salt used to make this ternary salt was of high purity and no peak occurring at 410°C appeared on the STA thermogram. Invariant transition temperatures for each peak at each heating rate are provided in Table 5.
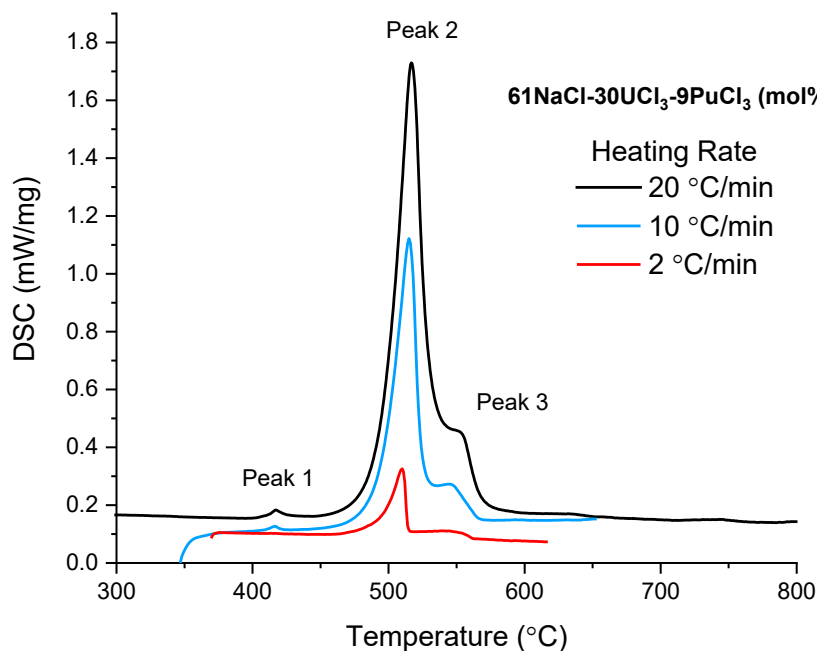

Figure 3. Thermograms for the ternary, 61NaCl-30UCl$_3$-9PuCl$_3$ (mol%) salt, using 20, 10, and 2°C min^{-1} heating rate.

Table 5. Invariant temperatures for each heating rate.

20°C min⁻¹	Peak 1 (Onset)	Peak 1	Peak 2	Peak 3 (Liquidus)	Peak 3 (Endset)
	°C	°C	°C	°C	°C
1	409.3	417.7	517.9	555.6	569.4
2	409.1	417.0	516.7	554.8	567.4
3	407.5	416.7	516.7	554.4	569.7
Average	408.6	417.1	517.1	554.9	568.8
Stdev	0.987	0.513	0.693	0.611	1.250
RSD, %	0.241	0.123	0.134	0.110	0.220
10°C min⁻¹	**Peak 1 (Onset)**	**Peak 1**	**Peak 2**	**Peak 3 (Liquidus)**	**Peak 3 (Endset)**
1	410.1	416.8	514.7	550.4	563.9
2	410.2	416.2	515.0	547.2	566.0
3	410.3	416.0	514.6	546.4	562.4
Average	410.2	416.3	514.8	548.0	564.1
Stdev	0.100	0.416	0.208	2.117	1.808
RSD, %	0.024	0.100	0.040	0.386	0.321
2°C min⁻¹	**Peak 1 (Onset)**	**Peak 1**	**Peak 2**	**Peak 3 (Liquidus)**	**Peak 3 (Endset)**
1	NA	NA	510.4	552.7	561.4
2	NA	NA	509.5	551.4	562.6
3	NA	NA	510.4	548.4	562.1
Average	—	—	510.1	550.8	562.0
Stdev	—	—	0.520	2.205	0.603
RSD, %	—	—	0.102	0.400	0.107

NA – Was not discernible on the heating curve.

The stability, or resistance to volatilization, of the ternary salt was determined using the STA. A baseline was run using an empty sample and reference crucible, each containing a lid with a small hole in the center. An aliquot of the ternary salt was weighed and loaded into the sample crucible. The sample crucible and empty reference were run to the same temperature program as the baseline. This was repeated for each heating rate. Mass change curves for the ternary $NaCl$-UCl_3-$PuCl_3$ salt are shown in Figure 4A–F. An initial mass loss between 0.8 and 1.29% was observed for each sample between 30 to 600°C on the initial heating step. After the initial heating step up to 800°C, no further mass loss occurred for the 20°C min⁻¹ sample, and the result was similar for the samples run at other heating rates.

There are numerous reasons a sample may lose mass. One possibility is that the ternary was contaminated with moisture coming from the salt contaminated with residual ethanol (clean agent), leading to the presence of a uranium-oxide compound. The presence of UO_2, UO_3, or U_3O_8 in the ternary salt is supported in the orange color of the salt ingot observed in Figure 2E. Another option is that since the decomposition of UO_3 to U_3O_8 has been reported to occur between 400 and 650°C (Thein and Bereolos 2000), a decomposition (i.e., mass loss) was observed in the three samples reported in Figure 4.
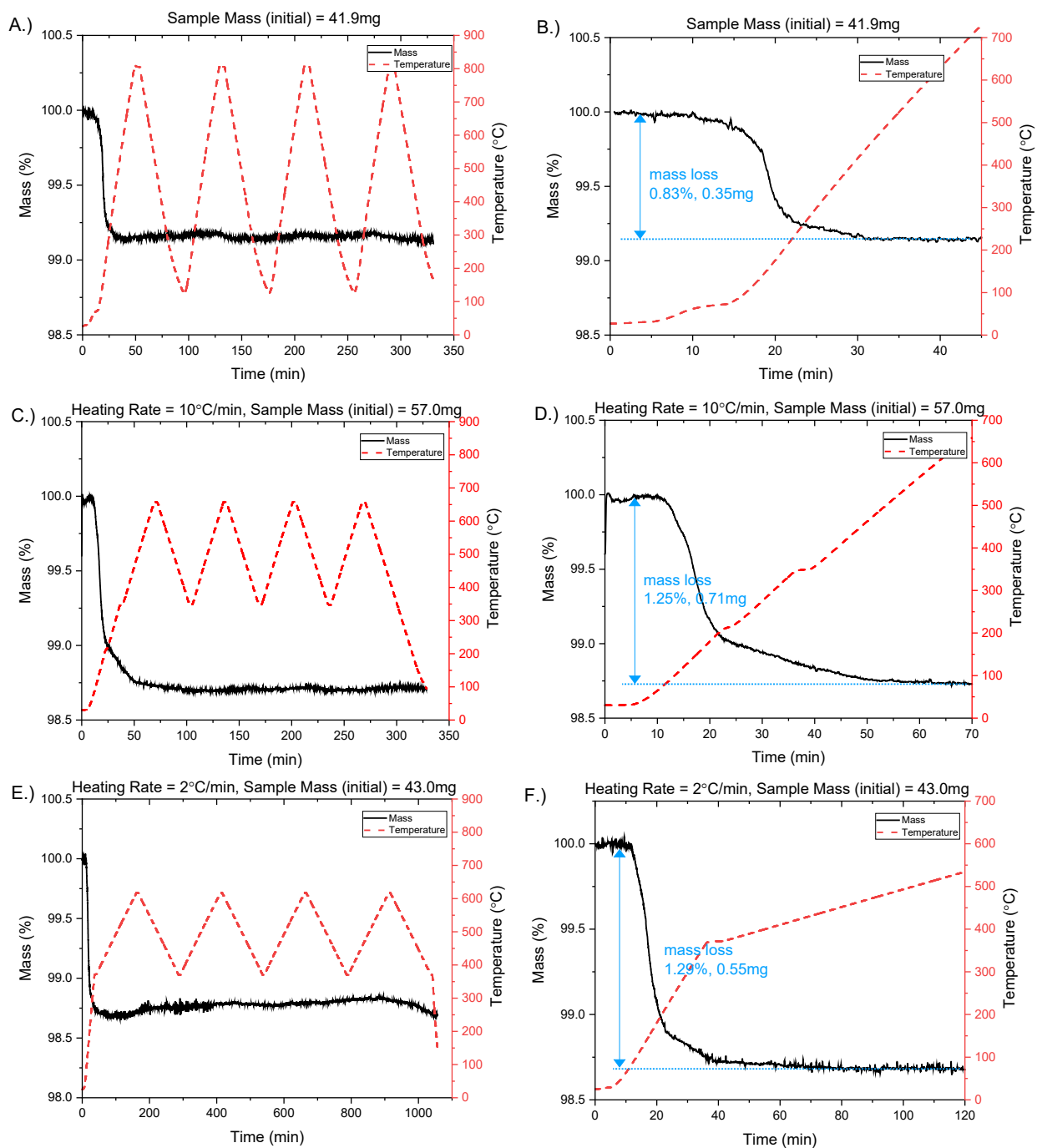
Figure 4. Mass change curves for the 61NaCl–30UCl$_3$–9PuCl$_3$ (mol%) salts. A.) salt run at 20°C min^{-1}, B.) first heating segment at 20°C min^{-1}, C.) salt run at 10°C min^{-1}, D.) first heating segment at 10°C min^{-1}, E.) salt run at 2°C min^{-1}, and F.) first heating segment at 2°C min^{-1}.

2.2.3   Density

The density of the molten NaCl-UCl$_3$-PuCl$_3$ salt was studied at temperatures between 550 and 850°C. A plot of the density measurements taken for the ternary 61NaCl–30UCl$_3$–9PuCl$_3$ (mol%) salt is shown in Figure 5. Experimental results show that the density of the molten salt decreased linearly as temperature increased. Therefore, a linear fit (dashed line) was used to generate an equation for density as a function of temperature, shown in Figure 5. In addition to the experimental density measurements taken at INL, density was also determined by using ab initio molecular dynamic (AIMD) simulations performed at PNNL by collaborator Dr. Manh Thuong Nguyen.
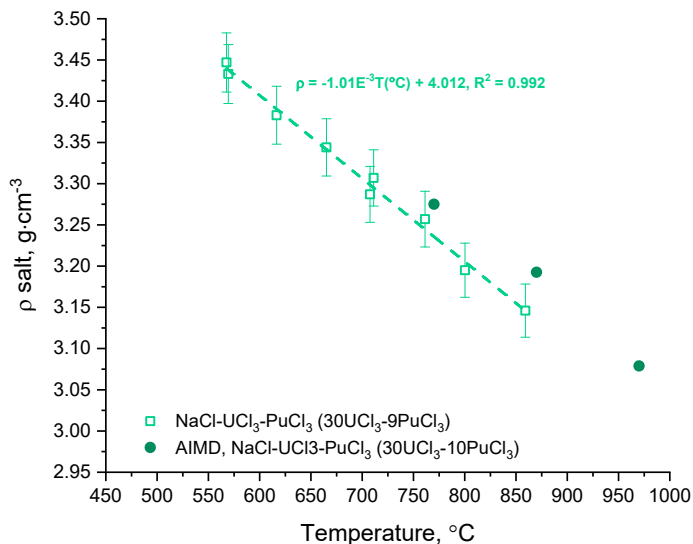
Figure 5. Experimental (open squares) and modeled (closed circles) density data for a ternary salt, 61NaCl–30UCl$_3$–9PuCl$_3$ (mol%).

The ternary salt investigated in this work is compared to other binary actinide salts including the 64NaCl–36PuCl$_3$ (mol%) investigated in FY-22 by the MSR Campaign and the 67NaCl–33UCl$_3$ (mol%) eutectic salt. It can be seen in Figure 6 that the density of the ternary salt is higher than that of the binaries. This is logical because the ternary salt has a higher total actinide (Ac = UCl$_3$ and PuCl$_3$) concentration. Combining the concentration of actinides yields a pseudo binary salt of 61NaCl–39AcCl$_3$ (mol%).

Figure 6. Summary of experimental (open squares) and AIMD (closed circles) density measurements for several actinide-bearing chloride salts.

3. BINARY NaCl-PuCl$_3$ EUTECTIC POST-FLOW LOOP OPERATIONS SALT

In 2020, INL and TerraPower collaborated on operating a NaCl-PuCl$_3$ natural convection salt-flow loop. As part of the collaboration, INL staff synthesized the NaCl-PuCl$_3$ salt and operated the flow loop for just over 1,000 hr in the argon atmosphere hot cell located 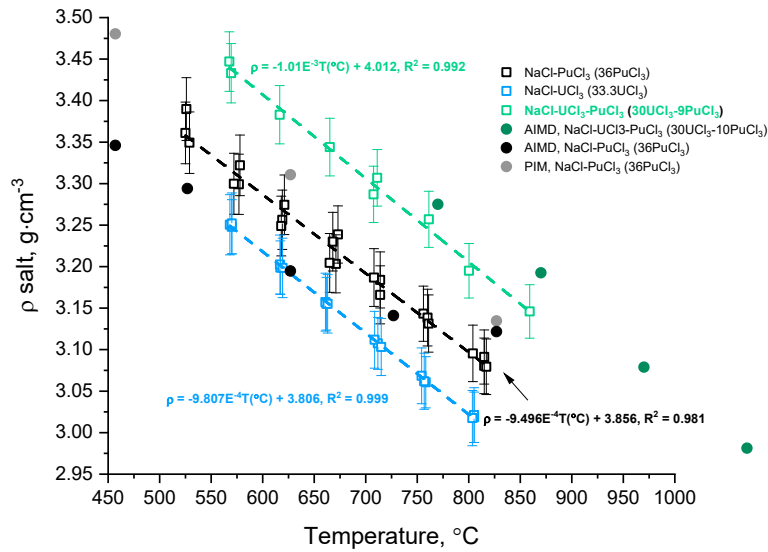in the Fuel Conditioning Facility (FCF) at INL. Additionally, in FY-22, INL, under the MSR Campaign, determined the thermal properties of NaCl-PuCl$_3$ and published a joint peer-reviewed journal article in the *Journal of Molecular Liquids* on the salt synthesis (TerraPower) and thermal properties (MSR Campaign), titled "Synthesis and thermophysical property determination of NaCl-PuCl$_3$ salts" (Karlsson, Middlemas, et al. 2023).

Once flow-loop operations were complete, the flow loop was drained of NaCl-PuCl$_3$ salt, then disassembled to examine the corrosion on the material of construction. This project was the first time ever that a Pu-based salt had been circulated in a flowing loop. Examining the post-operations flow-loop salt was out of scope for TerraPower but presented a unique opportunity for the MSR Campaign to investigate a fuel salt with possible corrosion products. Therefore, the MSR Campaign retrieved 40 g of NaCl-PuCl$_3$ salt after flow-loop operations for elemental/isotopic analysis and thermal property determination. The process of removing salt from the primary tank, as shown in Figure 7, was tedious, as the salt was removed using a dip sampler, collecting about 1 g of salt per dip. The post-flow loop salt is remarkable because it could potentially contain corrosion products, oxygen or moisture contamination, and contamination from handling the salt within the FCF hot cell and precursor facility transfer. Additionally, this is a non-surrogate, "real-world" salt, similar to what could be expected in an MSR, only without fission products.
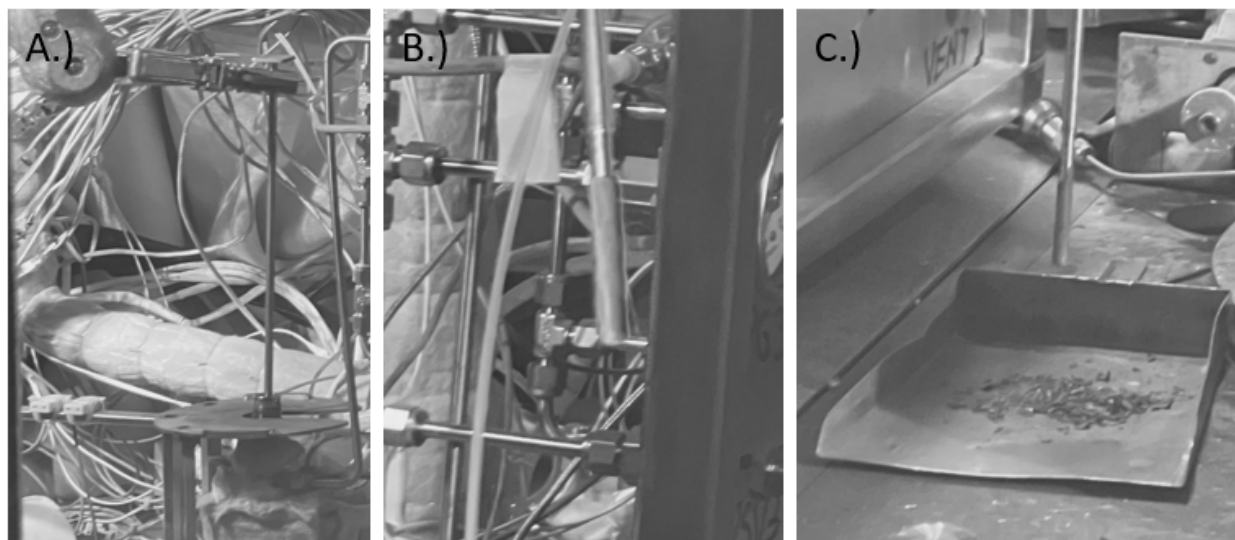
Figure 7. NaCl-PuCl$_3$ salt being removed from the flow loop (pictures in greyscale). A) remote operations using a dip sampler to "freeze" and remove salt, B) frozen salt of dip sampler, and C) chunks of salt after being removed from the dip sampler.

3.1 Methods

3.1.1 Elemental and Isotopic Analysis

Once the 40 g of salt were collected, three approximately 1 g samples were transferred to the ARL for elemental and isotopic analysis while the remaining salt was transferred to the Fuel Manufacturing Facility for density and melting temperature experiments prior to storage. In the ARL, the salt samples were weighed and dissolved using six molar hydrochloric acid (6M HCl), then one drop of hydrofluoric acid (HF) was added; the samples were heated, and a final addition of 1 mL of 16 M nitric acid (HNO$_3$) was made, as can be seen in Figure 8. The samples were diluted for isotopic analysis on the inductively coupled plasma optical mass spectrometer (ICP-MS). The diluted samples were also counted on the gamma spectrometer to determine the americium (^{241}Am) concentration to distinguish between ^{241}Am and ^{241}Pu isotopes and the cesium (^{131}Cs) concentration to determine if the post-flow-loop salt had been contaminated by the FCF hot-cell atmosphere.
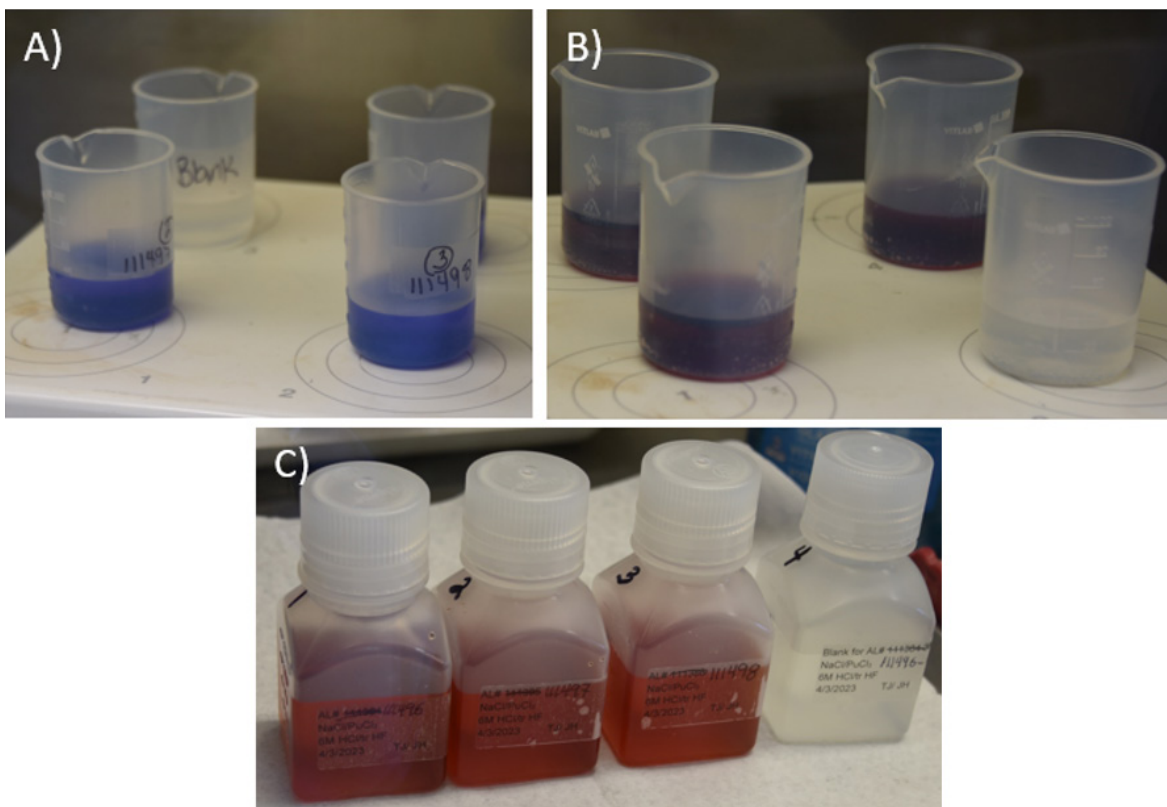
Figure 8. Dissolved post-flow-loop-salt samples. A) dissolved samples after 6 M HCl addition, B) dissolved samples after HF and HNO_3 addition, and C) parent sample, first dilution from bulk dissolver solution.

Before trace analysis of impurities could be carried out by inductively coupled-optical emissions spectrometry (ICP-OES), a portion of the parent solution was chemically separated to remove the Pu from the matrix. Pu has a rich emission spectrum, which can interfere with determining other analytes of interest, particularly if they are present in only trace quantities. The separations were carried out using auto-gas-pressurized extraction chromatography (auto-GPEC). Once the sample was loaded into the auto-GPEC, a pressurized-gas line pushed the sample through the chromatographic column, and the eluent was collected on the other side. To remove the Pu, a tetra-valent actinide (TEVA, Eichrom) 100–150 μm resin was used as the stationary phase.

3.1.2 Melting Temperature

Refer to Section 2.1.2.

3.1.3 Density

Refer to Section 2.1.3.

3.2 Results

3.2.1 Elemental and Isotopic Analysis

Analytical results from the ICP-OES, ICP-MS, and gamma spectroscopy for the pre-flow loop salt, $64NaCl – 36PuCl_3$ (mol%), are shown in Table 6 alongside the analytical results for the post-flow-loop salt. ICP data did not detect "typical" corrosion elements, except for Al detected by ICP-OES and niobium (Nb), cobalt (Co), Ni, and zirconium (Zr) detected by ICP-MS. Prior to flow loop operations, the composition of the primary fuel salt was verified to be $64NaCl–36PuCl_3$ (mol%). Further analysis by ICP-

13

MS showed a decrease in the Pu and all actinide isotope concentrations. This makes sense due to the higher magnesium (Mg) values. According to ARL data, there were 7.133 g $MgCl_2$ (12.902g of $MgCl_2$-NaCl eutectic flush salt) in 100 g of the fuel salt, which translates to a salt composition of $10MgCl_2$-$64NaCl$-$26PuCl_3$ (mol%). By mass balance, there was about 3% excess NaCl, meaning that there may have been a Pu-Ni intermetallic layer on the loop walls. Scanning electron microscopy and melting point analysis will provide further information. The Na values had an uncertainty of +/-10%, potentially yielding misleading mass balance results.

Table 6. Elemental and isotopic results for the pre- and post-flow-loop salt.

ICP-OES			ICP-MS		
Element	Pre-Flow Loop	Post-Flow Loop	Element	Pre-Flow Loop	Post-Flow Loop
—	ug/g	ug/g	—	ug/g	ug/g
Al	NR	163	Co	NR	1.93
Ba	<15	<5	Cr	<20	420
Cr	<20	<15	Cu	NR	<4
Fe	73	<30	Ni	<60	21
K	<220	<200	Zr	NR	11.4
Li	<45	<25	Mn	NR	<3
Mg	NR	18100	Mo	<3	<1
Mn	<15	<5	Nb	NR	0.704
Na	94900	105533	Sr-88	8.06	<0.6
Ni	<60	<20	Ta	NR	<20
Pr	<84	<85	Ti	NR	<30
Zn	NR	<50	Mo-100	<30	<0.1
Zr	<80	<55	M/Z-137	<2	<1
			Ba-138	11.7	<4
			Pr	NR	5.83
Gamma Spectroscopy			U-234	60.4	8.8
Element	Pre-Flow Loop	Post-Flow Loop	U-235	406	70.4
	ug/g	ug/g	U-236	283	41.3
Am-241	4113.186	4390.315	U-238	246	222
Cs-134	<1	<9	Np-237	212	145
Cs-137	<1	<10	Pu-239	469000	374000
			Pu-240	91600	72167
			M/Z-241	6040	4970
			M/Z-242	1960	1683

NR = not requested for analysis

Prior to running the primary salt ($NaCl$-$PuCl_3$ eutectic) through the flow loop, a rinse salt ($57NaCl$–$43MgCl_2$ (mol%)) was used to condition the flow loop and remove any residual oxides or contamination that might be in the loop from construction. Additionally, $NaCl$-$MgCl_2$ was used to make freeze plugs in

the loop to prevent the primary salt from leaking into the rinse tank. Because the analytical data determined the presence of $MgCl_2$ in the primary salt, it can be concluded that there was interaction between the primary and rinse salts. During flow-loop operations, there may have been some "pockets" of rinse salt that combined with the primary salt. Additionally, the primary salt could have interacted with (melted) salt from the freeze plugs.

The oxide or moisture within the flow-loop salt could not be directly quantified; however, a 99.5% mass balance provided by the analytical data indicated that there was minimal or no moisture or oxygen contamination. The loop also operated for 1,000 hr, and, if moisture was present, corrosion products would have been likely to form rapidly. The initial primary and rinse salts were determined to be of high purity by DSC analysis, and a significant effort was made in the design of the salt loading devices not to expose the salt to the atmosphere within the FCF hot cell. The appearance of the initial flow-loop salt ($64NaCl–36PuCl_3$ (mol%) eutectic) is shown in Figure 9A, while the post-flow-loop salt ($10MgCl_2–64NaCl–26PuCl_3$ (mol%)) is shown in Figure 9B. As can be seen, the salt darkened during flow loop operations. Darkening of pure $NaCl-PuCl_3$ eutectic is not uncommon, but the blue-green color typically reappears after heat treatment; however, the blue-green color did not return to the post-flow-loop salt, perhaps due to the inclusion of the rinse salt ($NaCl-MgCl_2$).
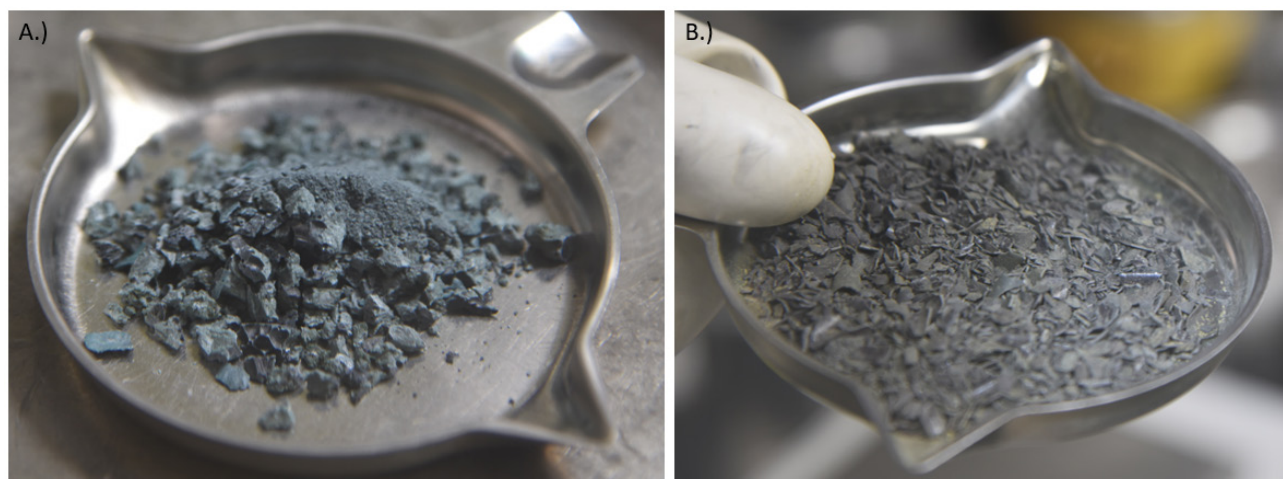

Figure 9. Images of flow loop salt. A.) Pre-flow loop operation and B.) post-flow loop operation.

3.2.2 Melting Temperature

The thermogram of the post-flow-loop salt is show in Figure 10. Incorporating the initial flow-loop salt ($64NaCl–36PuCl_3$ (mol%)) with eutectic $NaCl-MgCl_2$ rinse salt resulted in a post-flow-loop salt with a lower onset melting temperature. The liquidus occurred at 449°C in the pre-flow loop salt; however, the post-flow-loop salt had an onset melting temperature of 398°C. Three peaks can be observed in Figure 10, all occurring within 30°C of the onset temperature, suggesting the resulting ternary, post-flow loop salt composition $10MgCl_2–64NaCl–26PuCl_3$ (mol%) is very near a ternary eutectic composition.
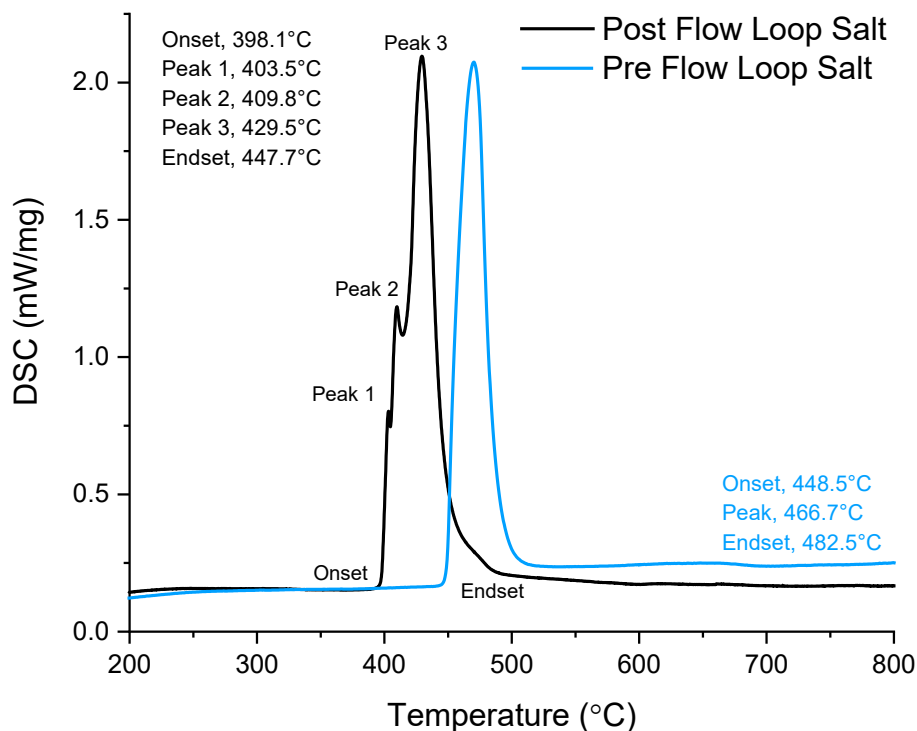
Figure 10. Thermogram for post- and pre-flow loop salt collected using a heating rate of 20°C min^{-1}.

3.2.3   Density

Composition (Table 6), color change (Figure 9), and melting temperature (Figure 10) were not the only properties that changed during flow-loop operations. Figure 11 shows the experimentally determined density values of the primary salt after 1,000 hr of flow-loop operation. The density of the post-flow-loop salt decreased by approximately 10% compared to the initial 64NaCl–36PuCl$_3$ (mol%) eutectic primary salt, which also caused a volume expansion of the primary salt. While density does not affect corrosion, these results provide a data point for what MSR operators and designers can expect when unintended mixing of the flush (rinse) salt occurs with the fuel (primary) salt. Sufficient head space must be incorporated into the design of MSRs to allow for expansion of the fuel salt with temperature and unintended blending of flush salt.
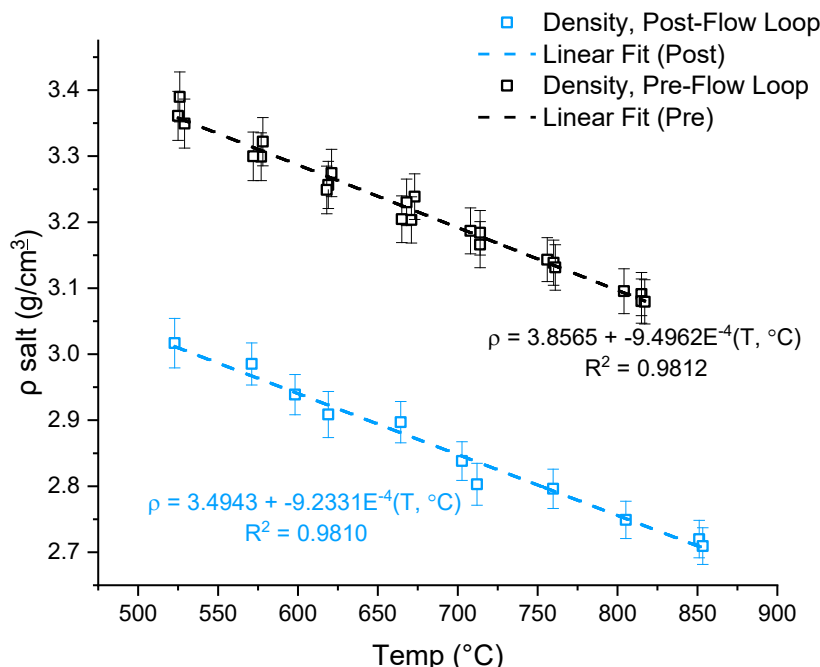
Figure 11. Experimental density as a function of temperature obtained on the primary flow-loop salt. Pre-flow-loop primary salt, 64NaCl–36PuCl$_3$ (mol%) eutectic shown in open black squares and post-flow-loop primary salt 10MgCl$_2$–64NaCl–36PuCl$_3$ (mol%) shown in open blue squares.

4.   CONCLUSIONS

This work had two key objectives for thermophysical properties: (1) study the extent to which impurity-driven variations, in this case a bounding scenario where transuranic fission products, represented by PuCl$_3$, build up in a 67NaCl-33UCl$_3$ (mol%) fuel salt and (2) examine a potential fuel salt, 64NaCl–36PuCl$_3$ (mol%) after 1,000 hr of operation in a natural convection micro-loop (TerraPower) to quantify corrosion products that may build up in the salt or cause reduction-oxidation reaction with fuel salt constituents, such as Pu.

A conservative assumption, or worst-case scenario, for fission product buildup was investigated by the addition of PuCl$_3$ to a 67NaCl–33UCl$_3$ (mol%) eutectic fuel salt, resulting in a ternary salt with a composition of 61NaCl–30UCl$_3$–9PuCl$_3$ (mol%) This salt was amalgamated and homogenization prior to density and melting temperature determination. The density of the ternary salt increased compared to the NaCl-UCl$_3$ eutectic due to the increased actinide loading with PuCl$_3$. Additionally, the liquidus temperature of quasi-eutectic NaCl-UCl$_3$ increased due to the addition of PuCl$_3$. Because the melting temperature of the NaCl-PuCl$_3$ binary systems is, in general, lower than that of the NaCl-UCl$_3$ binary system, it was predicted that addition of PuCl$_3$ to the NaCl-UCl$_3$ eutectic salt would lower the liquidus temperature; this, however, was not the case. Adding PuCl$_3$ to NaCl-UCl$_3$ eutectic increased the liquidus temperature to approximately 550°C. The presence of PuCl$_3$ did appear to suppress the liquids temperature when compared to the binary 61NaCl–39UCl$_3$ (mol%), which has a liquidus temperature of 576°C. When blending and homogenizing the ternary 61NaCl–30UCl$_3$–9PuCl$_3$ (mol%) salt, a thin layer of orange material appeared on the salt. Mass change curves from the TGA observed an initial mass loss between 0.8 and 1.29% for each sample between 30 and 600°C on the initial heating step. Both the orange color and mass loss may indicate the presence of a small concentration (~1wt%) of UO$_3$ in the ternary salt sample.

A unique opportunity existed to analyze a potential fuel salt, 36NaCl–64PuCl$_3$ (mol%), after exposure to corrosion testing in a natural circulation flow loop. In this report, the fuel salt was referred to as primary salt in flow-loop operations. Analyzing the post-flow-loop salt and comparing it to the initial salt (pre-flow loop) showed that after 1,000 hr of operation, the salt contained small amounts of Al, Nd, Ni, Co, and Zr. Mg (in the form of MgCl$_2$) was not initially detected by the ICP-OES in the pre-flow-loop salt; however, approximately 10 mol% of MgCl$_2$ was shown to be in the resulting post-flow-loop salt. The rinse salt for the flow loop was 57NaCl–43MgCl$_2$ (mol%) eutectic and likely blended with the primary NaCl-PuCl$_3$ salt during operation, resulting in a post-flow-loop-salt having a composition of 10MgCl$_2$–64NaCl–26PuCl$_3$ (mol%). Adding the MgCl$_2$-NaCl to the primary salt decreased the density of the primary flow loop salt by approximately 10% and lowered the onset melting temperature by approximately 50°C.

This report satisfies milestone M3AT-23IN0705021, *Draft Journal Article on NaCl-UCl$_3$-PuCl$_3$ properties*. The research included in this report will be used in two journal articles. The contents of Section 2 will be included in a joint manuscript with Dr. Manh Thuong Nguyen of PNNL with the tentative title, "A combined computational experimental study of NaCl–UCl$_3$–PuCl$_3$ molten salt mixtures." The contents described in Section 3 will be included in a joint publication with TerraPower with a tentative title, "Analysis of an Actinide Fuel Salt and Micro-Loop after 1000 Hours of Micro-Loop Operating Hours."

5.   REFERENCE

ASTM. 2018. Standard Test Method for Temperature Calibration of Differential Scanning Calorimeters and Differential Thermal Analyzers. West Conshohicken, PA: ASTM International, ASTM E967-18.

Compere, E. L., S. S. Kirslis, E. G. Bohlmann, F. F. Blankenship, and W. R. Grimes. 1975. Fission product behavior in the Molten Salt Reactor Experiment. United States.

Duemmler, Kai, Yuxiao Lin, Michael Woods, Toni Karlsson, Ruchi Gakhar, and Benjamin Beeler. 2022. "Evaluation of thermophysical properties of the LiCl-KCl system via ab initio and experimental methods." *Journal of Nuclear Materials* 559:153414. doi: https://doi.org/10.1016/j.jnucmat.2021.153414.

Faure, Bastien, and Timothée Kooyman. 2022. "A comparison of actinide halides for use in molten salt reactor fuels." *Progress in Nuclear Energy* 144:104082. doi: https://doi.org/10.1016/j.pnucene.2021.104082.

Hidnert, Peter. 1957. "Thermal Expansion of Some Nickel Alloys." *Journal of Research of the National Bureau of Standards* 58 (2):89 - 92.

IAEA. 2021. *The Potential Role of Nuclear Energy in National Climate Change Mitigation Strategies*. Vienna: INTERNATIONAL ATOMIC ENERGY AGENCY.

Karlsson, Toni, Cynthia Adkins, Ruchi Gakhar, James Newman, Steven Monk, and Stephen Warmann. 2023. "Phase Behavior of the Ternary NaCl-PuCl$_3$-Pu Molten Salt." *Journal of Nuclear Fuel Cycle and Waste Technology*:55-64.

Karlsson, Toni Y., Scott C. Middlemas, Manh-Thuong Nguyen, Michael E. Woods, Kevin R. Tolman, Vassiliki-Alexandra Glezakou, Steven D. Herrmann, Juliano Schorne-Pinto, Ryan D. Johnson, Shawn E. Reddish, Stephen A. Warmann, and Patricia D. Paviet. 2023. "Synthesis and thermophysical property determination of NaCl-PuCl3 salts." *Journal of Molecular Liquids* 387:122636. doi: https://doi.org/10.1016/j.molliq.2023.122636.

Karlsson, Toni Y., Scott C. Middlemas, Michael Ellis Woods, Kevin R. Tolman, Ryan D. Johnson, Shawn E. Reddish, Stephen A. Warmann, Vanda Glezakou, and Manh Thuong Nguyen. 2022. Synthesis and Thermophysical Property Determination of NaCl-PuCl3 Salts. United States.

Raiman, Stephen S., and Sangkeun Lee. 2018. "Aggregation and data analysis of corrosion studies in molten chloride and fluoride salts." *Journal of Nuclear Materials* 511:523-535. doi: https://doi.org/10.1016/j.jnucmat.2018.07.036.

Sooby, E. S., A. T. Nelson, J. T. White, and P. M. McIntyre. 2015. "Measurements of the liquidus surface and solidus transitions of the NaCl–UCl3 and NaCl–UCl3–CeCl3 phase diagrams." *Journal of Nuclear Materials* 466:280-285. doi: https://doi.org/10.1016/j.jnucmat.2015.07.050.

Sridharan, K., and T. R. Allen. 2013. "12 - Corrosion in Molten Salts." In *Molten Salts Chemistry*, edited by Frédéric Lantelme and Henri Groult, 241-267. Oxford: Elsevier.

Thein, S. M., and P. L. Bereolos. 2000. Thermal Stabilization of $^{233}UO_2$, $^{233}UO_3$, and $^{233}U_3O_8$. Oak Ridge, Tennessee 37831-6285: Oak Ridge National Laboratory.

Vigier, Jean-François, Annabelle Laplace, Catherine Renard, Manuel Miguirditchian, and Francis Abraham. 2016. "Uranium (III) precipitation in molten chloride by wet argon sparging." *Journal of Nuclear Materials* 474:19-27. doi: https://doi.org/10.1016/j.jnucmat.2016.03.005.